Synthesis and π-Hole vs. π Effects of Pt(II) Complexes with Pentafluorophenyl and Phenyl-Substituted Bipyridines

Akiko Hori [1,*] , Yuta Takeuchi [1], Tadashi Kawasaki [1], Naoki Toyama [2], Hidetaka Yuge [2] and Takashi Hiroi [1]

[1] Department of Applied Chemistry, Graduate School of Engineering and Science, Shibaura Institute of Technology, Fukasaku 307, Minuma-ku, Saitama 337-8570, Japan; thiroi@shibaura-it.ac.jp (T.H.)

[2] Department of Chemistry, School of Science, Kitasato University, Kitasato 1-15-1, Minami-ku, Sagamihara 252-0373, Japan; yuge@kitasato-u.ac.jp (H.Y.)

* Correspondence: ahori@shibaura-it.ac.jp; Tel.: +81-48-720-6350

Abstract: Four types of perfluoroarene-substituted and the corresponding non-fluorinated Pt(II) complexes, [PtCl$_2$L] (L = **1** and **2**), were prepared with 4,4′-bis(pentafluorophenyl)-2,2′-bipyridine (**1a**), 4,4′-diphenyl-2,2′-bipyridine (**1b**), 4,4′-bis(2-pentafluorophenylethynyl)-2,2′-bipyridine (**2a**), and 4,4′-bis(2-phenylethynyl)-2,2′-bipyridine (**2b**), respectively, to understand the role of perfluoroaromatic substitution and acetylene linkers on molecular structures and their induced supramolecular associations. The pentafluorophenyl groups lead to significant changes in electron distribution within the Pt(II) complexes, notably causing absorption bands to red-shift due to a metal-to-ligand charge transfer from nucleophilic platinum ions and demonstrating stabilization effects on the bands by fluorination in experimental and theoretical studies. The results of altering electron density and reducing the metal's nucleophilic tendencies through fluorination and the use of an acetylene linker are discussed, accompanied by crystal structures, the corresponding Hirshfeld surface analysis, and DFT calculations.

Keywords: bipyridine derivative; electrostatic interaction; fluorine; Hirschfeld surface analysis; platinum

1. Introduction

The exploration of charge distribution and its resultant electrostatic interactions within aromatic compounds stands at the forefront of chemical research due to its critical role in dictating the intramolecular electronic and intermolecular aggregated states of molecules [1–6]. The intricate behavior of charges induced by fluorine not only determines the intrinsic properties of molecules but also their behavior in a plethora of chemical reactions and applications, from organic electronics to pharmaceuticals [7–9]. In the realm of our research, we have delved into the study of aromatic fluorine compounds [10–14], a category known for its significant impact on chemical compounds due to the electron-withdrawing nature imparted by the fluorine substitutions. Aromatic fluorine molecules, exemplified by entities such as pentafluorophenyl groups [1,15–17], and heterocyclic molecules like those containing triazine rings [18] are distinguished as π-hole molecules [19–26]. This designation comes from their ability to exhibit regions with positive electrostatic potential, known as π-holes, resulting from the distribution of electron density. The presence of π-holes as substituents on molecules introduces a fascinating dimension to the study of intramolecular charge distribution. It dramatically influences the molecule's electronic environment, paving the way for the emergence of novel intermolecular interactions. These interactions are not merely of academic interest; they have profound implications for the development of new materials and the understanding of molecular dynamics at a fundamental level. On the other hand, the curiosity extends to bipyridine derivatives containing aromatic molecules. Bipyridine and its derivatives have garnered attention due to their versatile application potential, ranging from catalysis to material science [27,28]. The ability

of these molecules to coordinate with Pt(II) ions opens innovative research fields [29–32]. However, despite the interest in and development of coordination compounds reported in the recent literature, those featuring acetylene cross-linking are still lagging behind as there are still few reports [33–40]. The use of an acetylene linker offers the enticing prospect of modulating the aromatic plane's rotational barrier, significantly affecting the molecule's physical and chemical properties. Such fields prompted us to develop the investigation of phenylethynyl-substituted bipyridine to understand the supramolecular association of aromatic moieties [39] and the corresponding Pd(II) complex [40] through the electrostatic π-interactions.

In this study, we synthesized [PtCl$_2$L] (where L = **1** and **2**) and determined their structures and photophysical properties. Ligand **1** is directly linked, whereas ligand **2** is acetylene-linked between the aromatic rings, such as the pentafluorophenyl and phenyl groups, and the bipyridine moiety (Scheme 1). This report discusses the relationship between electron surface potential (ESP) and induced intermolecular interactions, as revealed by a detailed crystal structure analysis of [PtCl$_2$**1a**]•CHCl$_3$, [PtCl$_2$**1b**], [PtCl$_2$**2a**]•CH$_2$Cl$_2$, and [PtCl$_2$**2b**]•0.5C$_6$H$_6$. This study reveals the contribution of charge distribution and electrostatic interactions within aromatic compounds by focusing on the synthesis and detailed analysis of [PtCl$_2$L] complexes. Through the synthesis of the complexes with direct and acetylenic bonds between bpy and aromatic groups, we delve into the subtle interplay of ESP, opening the manipulation of the molecular structure to achieve the desired electronic properties. Our findings enhance the understanding of how the control over intramolecular structure—achieved through the introduction of fluorine substituents and acetylene bridges—affects intermolecular interactions. This work not only fills a gap in the understanding of π-hole interactions in aromatic fluorine compounds but also paves the way for the development of novel materials with tailored electronic environments.
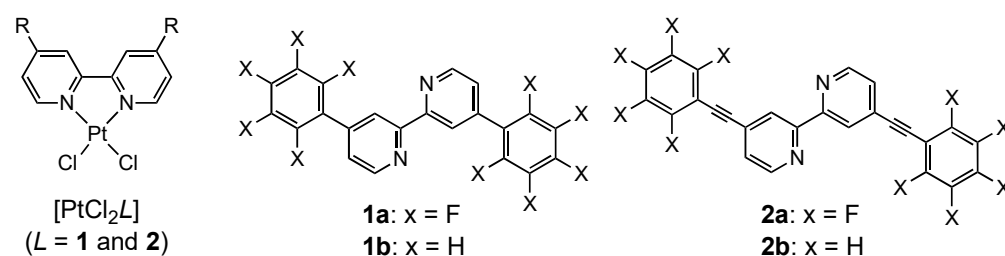
Scheme 1. Molecular structures of [PtCl$_2$L] and the corresponding ligands (**1** and **2**).

2. Materials and Methods

2.1. General

All the chemicals were of reagent grade and were used without further purification. The ^{1}H NMR spectral data were recorded on a JEOL ECS400 spectrometer (JEOL Ltd., Tokyo, Japan). The melting points were determined using a Yanako MP-500D melting point apparatus (Yanako, Kyoto, Japan). Mass data were obtained using GC-MS QP2010Plus (Shimadzu Co., Kyoto, Japan). UV-Vis spectra were measured using a JASCO V-660DS (JASCO Co., Tokyo, Japan). The results of the elemental analysis (EA) of C, H, and N were determined using a Perkin-Elmer PE2400 analyzer (PerkinElmer Japan G.K., Yokohama, Japan). Density functional theory (DFT) was used to simulate the energy levels of the molecular orbitals for the ground electronic states of [PtCl$_2$L] (L = **1** and **2**) as a gas state. The calculation was performed with the B3LYP method and LANL2DZ basis sets in Gaussian 16 software (HULINKS Inc., Tokyo, Japan) [41]. The ESP was calculated by DFT using the Spartan'20 package (V1.1.4) with ωB97X-D/6-31G* (Wavefunction Inc., Tokyo, Japan).

2.2. Preparations and Characterization

The compounds **1b**, **2**, and [PtCl$_2$(dmso)$_2$] were prepared following previously reported protocols [39,40]. 4,4′-Bis(pentafluorophenyl)-2,2′-bipyridine (**1a**) was prepared via Suzuki–Miyaura cross-coupling reaction. 4,4′-dibromo-2,2′-bipyridine (160 mg, 0.50 mmol),

pentafluorophenylboronic acid (250 mg, 1.2 mmol), Ag_2O (460 mg, 1.9 mmol), $K_3PO_4 \cdot H_2O$ (1.7 g, 8.0 mmol), and $[Pd(PPh_3)_4]$ (92 mg, 80 µmol) were combined in 30 mL of dimethyl-formamide under inert gas [42]. The mixture was stirred at 85 °C for 9 h. An aqueous solution of NH_4Cl was added to the reaction mixture, and the precipitate was obtained. The precipitate was purified using column chromatography (silica, $CHCl_3$:MeOH = 40:1) and GPC ($CHCl_3$) to yield a white powder of **1a**. Yield: 28%. mp: 240–241 °C. ^{1}H NMR (400 MHz, $CDCl_3$): δ 8.82 (d, 2H), 8.59 (s, 2H), 7.41 (d, 2H). GI-MS: m/z 488 [M[+]]. Elemental analysis: Calcd for $C_{22}H_6F_{10}N_2$ (%): C 54.12, H 1.24, N 5.74; found: C 54.32, H 1.24, N 5.88.

Complexes $[PtCl_2L]$ (*L* = **1** and **2**) were prepared in a single step using the corresponding ligands, e.g., **1a**, **1b**, **2a**, and **2b**, respectively, with $[PtCl_2(dmso)_2]$. To a solution of the corresponding ligand (0.01 mmol) in benzene (1 mL), a solution of $[PtCl_2(dmso)_2]$ (0.01 mmol) in DMSO (several drops) was slowly added. The reaction mixture was kept for several days at room temperature to obtain single crystals, which were suitable for X-ray crystallographic studies.

[PtCl2**1a**]: Yellow prismatic crystals. Yield 70%. mp 255 °C dec. ^{1}H NMR ($CDCl_3$, TMS): δ 9.94 (d, 2H), 8.09 (s, 2H), 7.72 (d, 2H). UV-Vis [CH_2Cl_2, λ nm (ε M^{-1} cm^{-1})]: 277 (28000), 322 (51200), 345 (20200), 427 (9100), 520sh (160). Elemental analysis: Calcd for $C_{22}H_6Cl_2F_{10}N_2Pt$ (%): C 35.03, H 0.80, N 3.71; found: C 35.36, H 0.66, N 4.02.

[PtCl2**1b**]: Pale orange block crystals. Yield 19%. mp 375 °C dec. ^{1}H NMR (400 MHz, dmso-d_6): δ 9.48 (d, 2H), 9.06 (s, 2H), 8.20 (d, 2H), 8.10 (dd, 4H), 7.66–7.59 (m, 6H). UV-Vis [CH_2Cl_2, λ nm (ε M^{-1} cm^{-1})]: 282 (30600), 300 (37700), 325 (47500), 418 (11700), 520sh (130). Elemental analysis: Calcd for $C_{22}H_{16}Cl_2N_2Pt$ (%): C 46.01, H 2.81, N 4.88; found: C 46.12, H 2.99, N 4.49.

[PtCl2**2a**]: Orange block crystals. Yield 85%. mp 315 °C dec. SI-MS: m/z 802 [M[+]], 767 [M-Cl], 731 [M-2Cl]. UV-Vis [CH_2Cl_2, λ nm (ε M^{-1} cm^{-1})]: 275 (66100), 320 (57400), 427 (11000), 520 (sh, 140). Elemental analysis: Calcd for $C_{26}H_6Cl_2F_{10}N_2Pt \bullet 0.25CH_2Cl_2$ (%): C 38.28, H 0.80, N 3.40; found: C 38.0, H 1.27, N 3.89.

[PtCl2**2b**]. Yellow plate crystals. Yield 91%. mp 330 °C dec. SI-MS: m/z 622 [M[+]], 586 [M-Cl], 551 [M-2Cl]. UV-Vis [CH_2Cl_2, λ nm (ε M^{-1} cm^{-1})]: 282 (48200), 299 (59200), 325 (74000), 418 (18200), 520 (sh, 150). Elemental analysis: Calcd for $C_{26}H_{16}Cl_2N_2Pt$ (%): C 50.17, H 2.59, N 4.50; found: C 50.07, H 2.62, N 4.42.

2.3. Crystal Structure Determination

The single crystal X-ray structures were determined using a Bruker SMART APEX CCD diffractometer (Bruker Japan, Yokohama, Japan) with a graphite monochrometer and Mo*K*α radiation (λ = 0.71073 Å) generated at 50 kV and 30 mA. All crystals were coated with paraton-N and measured at 100 K. Crystal data for $[PtCl_2L]$ (*L* = **1** and **2**) are summarized in Table 1. For all compounds, cell refinement and reduction were performed using the Bruker SAINT program, the structure solution was carried out with SHELXT, and the refinement was conducted using SHELXL [43]. Empirical adsorption corrections were applied using the SADABS program [44]. All non-hydrogen atoms were refined anisotropically unless otherwise stated, and hydrogen atoms were constrained at idealized positions, with the C–H distances set at 0.95 Å and U_{iso}(H) = 1.2 U_{eq}(C). These data can be obtained free of charge via http://www.ccdc.cam.ac.uk/structures/ (accessed on 28 April 2024).

Table 1. Crystal data and structure refinements for four types of Pt(II) complexes.

	[PtCl2**1a**]$\bullet$CHCl3	[PtCl2**1b**]	[PtCl2**2a**]$\bullet$CH2Cl2	[PtCl2**2b**]$\bullet$0.5C6H6
Chem. formula	$C_{23}H_7Cl_5F_{10}N_2Pt$	$C_{22}H_{16}Cl_2N_2Pt$	$C_{27}H_8Cl_4F_{10}N_2Pt$	$C_{29}H_{19}Cl_2N_2Pt$
F.W.	873.65	574.36	887.24	661.45
Crystal system	triclinic	tetragonal	monoclinic	monoclinic
Space group	*P*-1	P4$_3$2$_1$2	C2/*c*	P2$_1$/*c*
a [Å]	10.2586(15)	10.6663(12)	30.7010(12)	12.0428(10)
b [Å]	15.387(2)	10.6663(12)	11.5286(5)	11.6720(9)

Table 1. *Cont.*

	[PtCl$_2$1a]•CHCl$_3$	[PtCl$_2$1b]	[PtCl$_2$2a]•CH$_2$Cl$_2$	[PtCl$_2$2b]•0.5C$_6$H$_6$
c [Å]	17.188(3)	32.869(4)	19.9149(8)	17.4009(14)
α [°]	98.616(2)	90	90	90
β [°]	92.257(2)	90	129.13	104.562(1)
γ [°]	99.106(2)	90	90	90
V [Å^3]	2643.2(7)	3739.5(9)	5467.5(4)	2367.4(3)
Z	4	8	8	4
D_c [Mg m^{-3}]	2.195	2.040	2.156	1.856
μ [mm^{-1}]	5.904	7.800	5.616	6.174
F (000)	1648	2192	3360	1276
R_{int}	0.0232	0.0305	0.0199	0.0314
GOF	1.038	1.098	1.033	0.973
R [(I) > 2σ (I)]	0.0259	0.0363	0.0208	0.0241
wR ($F_o{}^2$)	0.0627	0.0873	0.0470	0.0509
CCDC No.	2346110	2346111	2346112	2346113

3. Results and Discussion

3.1. Preparation and Physical Properties of [PtCl$_2$L]

Complex [PtCl$_2$L] (L = **1** and **2**) was prepared in a one-step reaction using the corresponding ligands, e.g., **1a**, **1b**, **2a**, and **2b**, respectively, with [PtCl$_2$(dmso)$_2$]. To a solution of L (0.01 mmol) in benzene (1 mL), a solution of [PtCl$_2$(dmso)$_2$] (0.01 mmol) in DMSO (several drops) was slowly added. The reaction mixture was kept for several days at room temperature to yield single crystals suitable for X-ray crystallography and photophysical studies. Each CH$_2$Cl$_2$ solution of [PtCl$_2$L] was light yellow, and the crystals ranged in color from yellow to orange. Due to the low solubility of each complex, single crystals were directly obtained through natural concentrations from the reaction mixture, and no recrystallization was performed. Regarding the solution structure of each compound, [PtCl$_2$**1**] was quantitatively determined by NMR, while [PtCl$_2$**2**] was characterized by SI-MS due to its low solubility. The bulk composition of both compounds was determined by elemental analysis. The powdered form of these complexes showed yellow for [PtCl$_2$**1**] and vibrant orange for [PtCl$_2$**2**]. While differences in the redness of each crystal, which indicate the presence of polymorphism specific to the Pt(II) complexes [30,45,46], were observed during the concentration process, the major crystal structures were examined as described below.

The UV/Vis absorption spectra of **1** and its metal complex [PtCl$_2$**1**] were compared (Figure 1). Upon comparing ligands **1a** (black, solid line) and **1b** (black, dash line), they exhibited similar profiles due to mainly π-π* transitions within the 220–320 nm range, with 238 nm (ε = 35,100 M^{-1} cm^{-1}) and 290 nm (12,600 M^{-1} cm^{-1}) for **1a** and 250 nm (47,800 M^{-1} cm^{-1}) and 290 nm (12,600 M^{-1} cm^{-1}) for **1b**. The slight blue-shift observed in the perfluorinated ligand **1a** compared to **1b** can be attributed to the fluorine atoms at the *ortho*-positions affecting the planarity of the two aromatic groups, the pyridine and aromatic rings. Both ligands displayed a subtle absorption shoulder in the 320–400 nm range, aligning with the ultraviolet region, which corresponded to the color of ligand **1**; the shoulder peak was observed around 360 nm for **1,** and the ε of **1b** (450 M^{-1} cm^{-1}) was slightly larger than that of **1a** (110 M^{-1} cm^{-1}). The formation of the complex resulted in each absorption peak corresponding to the ligands showing a significant red-shift; the maximum absorption wavelength shifted from 238 nm to 322 nm for [PtCl$_2$**1a**] and from 250 nm to 325 nm for [PtCl$_2$**1b**] (see the green solid and dash lines, respectively). The result indicates a considerable change in conformation, likely due to the bipyridine component forming a discrete complex. As a general trend observed in platinum complexes [47–49], a d-π* charge transfer (MLCT) absorption band, indicative of platinum's characteristics, was observed beyond 427 nm, with the tail of the absorption band extending past 418 nm. The slight shift toward longer wavelengths in the fluorine-substituted complex was predicted to be due to the electrophilic effect of aromatic fluorine. Both complexes exhibited a minor transition shoulder at 520 nm, consistent with the complexes' reddish color.
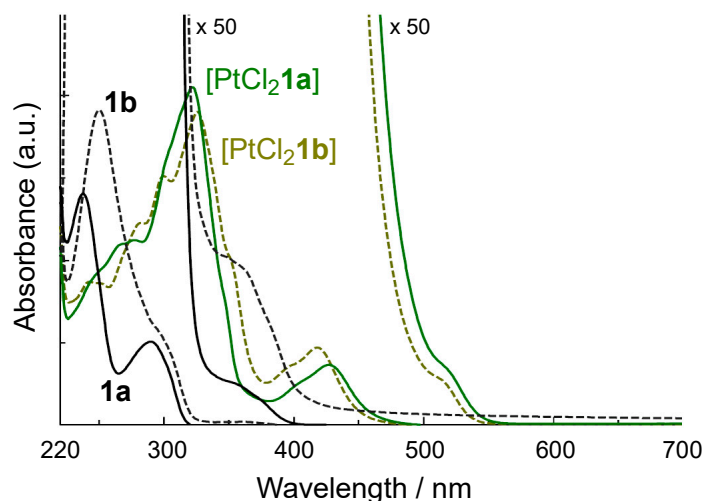
Figure 1. Absorption spectra of **1a** (black, solid), **1b** (black, dash), [PtCl$_2$**1a**] (green, solid), and [PtCl$_2$**1b**] (green, dash) in CH$_2$Cl$_2$ (0.02 mM) at r.t.

The absorption spectra of ligand **2** and its related metal complexes [MCl$_2$**2**] (M = Pt and Pd [40]) are shown in Figure 2. The peaks for ligand **2** indicate sharper vibrational transitions, featuring at least four strong bands at 265 (ε = 31,200 M^{-1} cm^{-1}), 282 (38,900 M^{-1} cm^{-1}), 298 (37,700 M^{-1} cm^{-1}), and 320 (sh, 9400 M^{-1} cm^{-1}) nm, attributed to π-π* transitions of the pyridine and pentafluorophenyl groups for **2a** (Figure 2a). The absorption maxima were observed at 268 (ε = 63,300 M^{-1} cm^{-1}), 290 (79,700 M^{-1} cm^{-1}), 302 (83,100 M^{-1} cm^{-1}), and 320 (sh, 40,400 M^{-1} cm^{-1}) nm for **2b**, corresponding to π-π* transitions between the pyridine and phenyl groups (Figure 2b). While the related Pt(II) and Pd(II) complexes show unique absorption bands around 280–320 nm aligning with the position observed for ligand **2**, new red-shifted peaks indicate the complex formation, around 330–350 nm for [MCl$_2$**2**]. The preservation of the ligand's absorption band in the ultraviolet region suggests that structural modifications within the bipyridine moiety due to acetylene crosslinking do not significantly alter the aromatic substituents. The remarkable peaks at 427 (ε = 11,000 M^{-1} cm^{-1}) and 520 nm (140 M^{-1} cm^{-1}) for [PtCl$_2$**2a**] and 418 (18,200 M^{-1} cm^{-1}) and 520 nm (150 M^{-1} cm^{-1}) for [PtCl$_2$**2a**] indicate the metal characteristics, i.e., the new peaks are expected as the MLCT is caused by the binding of a nucleophilic platinum ion to the bipyridine ligand, and its absorption band is slightly stabilized and red-shifted by fluorination. These findings elucidate the observed yellow color of [PdCl$_2$**2**] and the red color of [PtCl$_2$**2**].
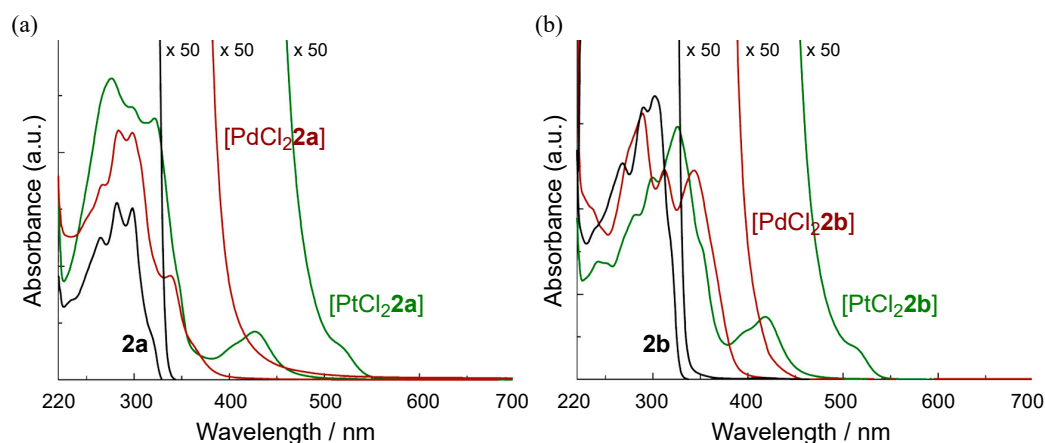

Figure 2. Absorption spectra of (**a**) **2a** and [MCl$_2$**2a**] and (**b**) **2b** and [MCl$_2$**2b**] (M = Pt and Pd) in CH$_2$Cl$_2$ (0.02 mM) at r.t.

3.2. Density Functional Theory Calculations of the Structures

Since the frontier molecular orbital energies play a crucial role in understanding the chemical characteristics of compounds, the energy levels of the ground electronic states of [PtCl$_2$L] were estimated by DFT calculations using the optimized isolated molecules. The highest occupied molecular orbital (HOMO) and the lowest unoccupied molecular orbital (LUMO) levels typically signify a molecule's propensity to donate electrons and its susceptibility to electrophilic properties and to electron affinity and the molecule's sensitivity to nucleophilic reactions, respectively, with the corresponding closest orbitals, e.g., HOMO−1 and LUMO+1. Thus, the HOMO-LUMO gap, determined by the energy difference between the HOMO and LUMO orbitals, qualitatively serves as a significant indicator of both molecular stability and color properties. Figure 3 shows the HOMO−1, HOMO, LUMO, and LUMO+1 orbitals of the complex, along with their corresponding energy values, and shows that the HOMO and HOMO−1 of the examined compounds are predominantly localized within the coordinative PtCl$_2$ core, whereas the LUMO and LUMO+1 are mainly distributed throughout the bipyridine moiety, clearly indicating the metal-to-ligand charge transfer (MLCT) and platinum's nucleophilicity. The HOMO energies of the four complexes, the perfluorinated and non-fluorinated complexes are around −6.4 and −5.9 eV, respectively, and the energy gap (ΔE/eV) increases in the sequence [PtCl$_2$**2a**] (2.39) < [PtCl$_2$**1a**] (2.52) < [PtCl$_2$**2b**] (2.63) < [PtCl$_2$**1b**] (2.76). The energy gap values from HOMO−1 to LUMO and from HOMO to LUMO+1 qualitatively account for the observed trend in the MLCT band between 400 and 500 nm as reported in the spectroscopic data. Despite the overall variance not being extensive, the observed differences clearly illustrate the enhanced stability of fluorinated compounds. This stability is attributed to the increased electron affinity and nucleophilic properties of the bipyridine moiety, which are amplified by the electron-withdrawing nature of the fluorine substitutions.
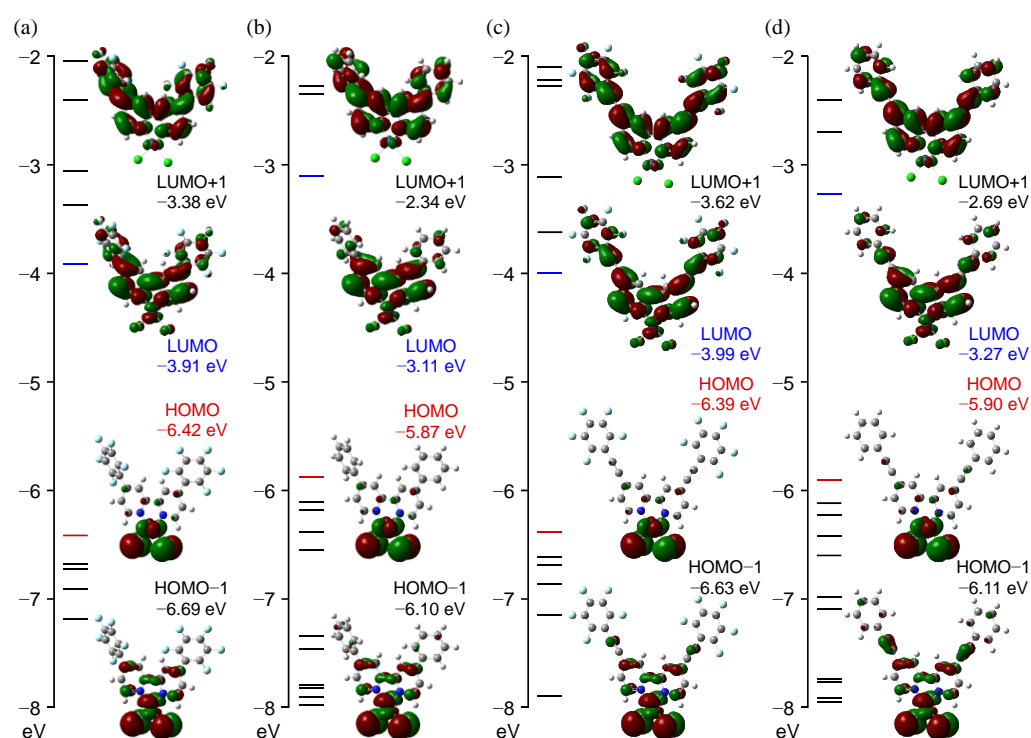

Figure 3. The energy levels in the vicinity of the frontier molecular orbitals, and the contour plots of the two highest occupied molecular orbitals (HOMO and HOMO−1) and the two lowest unoccupied molecular orbitals (LUMO and LUMO+1) of the complex [PtCl$_2$L] (L = **1** and **2**): (**a**) [PtCl$_2$**1a**], (**b**) [PtCl$_2$**1b**], (**c**) [PtCl$_2$**2a**], and (**d**) [PtCl$_2$**2b**] as optimized isolated molecule.

This electron distribution, the flow of electrons from the metal core (PtCl$_2$), to the coordination site (bpy) to the aromatic fluorine (C$_6$F$_5$), is also shown by ESP (Figure 4 and Table 2), which is calculated using the atomic coordinates from the crystal structure, as described below. The ESPs of the centroids (C_g) of the six-membered rings of pentafluorophenyl and phenyl groups are significantly different. The ESP values of the front and back surfaces of the two rings are +141, +141 kJ mol^{-1} and +138, +137 kJ mol^{-1}, respectively, for the pentafluorophenyl groups of [PtCl$_2$**1a**], −20, −15 kJ mol^{-1} and −20, −14 kJ mol^{-1} for the phenyl groups of [PtCl$_2$**1b**], +129, +129 kJ mol^{-1} and +126, +127 kJ mol^{-1} for the pentafluorophenyl groups of [PtCl$_2$**2a**] and −31, −27 kJ mol^{-1} and −25, −31 kJ mol^{-1} for the phenyl groups of [PtCl$_2$**2b**], showing π-holes with electron-deficient sites and π-conjugation with weak electrons, respectively. Introducing the pentafluorophenyl group results in the entire molecule's ESP changing to positive values approximately 30 kJ mol^{-1} and 20 kJ mol^{-1} for [PtCl$_2$**1**] and [PtCl$_2$**1**], respectively, indicating a decrease in electron-rich surfaces. This demonstrates that the electron-withdrawing nature of fluorine does not enhance the electron-rich regions of the molecule.
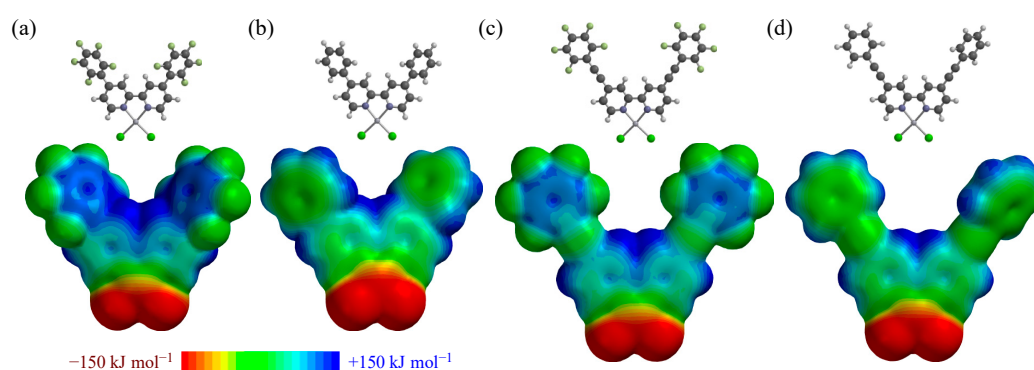

Figure 4. The energy potential maps of [PtCl$_2$*L*] (*L* = **1** and **2**): (**a**) [PtCl$_2$**1a**], (**b**) [PtCl$_2$**1b**], (**c**) [PtCl$_2$**2a**], and (**d**) [PtCl$_2$**2b**]. The color of the potential is shown between −150 kJ mol^{-1} (red) and +150 kJ mol^{-1} (blue), using atomic coordinates determined from the crystal structures.

Table 2. Selected ESP values (kJ mol^{-1}) of the complexes.

	[PtCl$_2$**1a**]	[PtCl$_2$**1b**]	[PtCl$_2$**2a**]	[PtCl$_2$**2b**]
Highest positive ESP (H)	+239.22	+210.32	+230.45	+211.75
Lowest negative ESP (Cl)	−277.61	−299.13	−278.62	−296.51
C_g on metal surface (Pt)	−94	−136	−103	−120
C_g of aromatic rings	+141, +141	−20, −15	+129, +129	−31, −31
C_g of pyridine rings	+94, +94	+59, +61	+91, +91	+69, +69

3.3. X-ray Crystallographic Study of [PtCl$_2$**1**]

The ORTEP views of the Pt(II) complexes in the crystal of [PtCl$_2$**1a**]•CHCl$_3$ and [PtCl$_2$**1b**] are shown in Figure 5a,b, respectively, with the numbering schemes. In the crystal of [PtCl$_2$**1a**]•CHCl$_3$, the asymmetric unit contains two whole complexes, namely complex-1 and complex-2, and two chloroform molecules (see Figure 6). The complex-1 comprises one Pt(II) ion, two Cl$^-$ ions, and one ligand **1a** to give a mononuclear complex (Figure 5a). The geometry around the metal center is pseudo-square planar, and the bond distances of Pt1–N1, Pt1–N2, Pt1–Cl1, and Pt1–Cl2 are 2.005(3), 2.005(3), 2.2973(9), and 2.2976(9) Å, respectively. The bipyridine planes (N1-C1-C2-C3-C4-C5, *ring-A* and N2-C12-C13-C14-C15-C16, *ring-C*) are highly flat [the torsion angle of N1-C5-C12-N2 is −0.7(4)°] due to Pt coordination. The pentafluorophenyl groups (C6-C7-C8-C9-C10-C11, *ring-B* and C17-C18-C19-C20-C21-C22, *ring-D*) are twisted with respect to the corresponding pyridine rings; the dihedral angles between *rings-A-B* and *C-D* are 44.32° and 43.35°, respectively. For complex-2 in the crystal, the geometry around the metal center is also

pseudo-square planar, and the bond distances of Pt2–N3, Pt2–N3, Pt2–Cl3, and Pt3–Cl4 are 2.010(3), 2.005(3), 2.2926(10), and 2.2996(11) Å, respectively. The bipyridine planes (*rings-A'* and *-C'*) are also flat, and the torsion angle of N3-C27-C34-N4 is 0.3(5)°. The pentafluorophenyl groups (C28-C33, *ring-B'* and C39-C44, *ring-D'*) are twisted with respect to the corresponding pyridine rings; the dihedral angles between *rings A'-B'* and *C'-D'* are 43.99° and 45.45°, respectively. Each structure is similar and presented in reflectional symmetry due to the steric hindrance of *ortho*-substituted fluorine atoms.
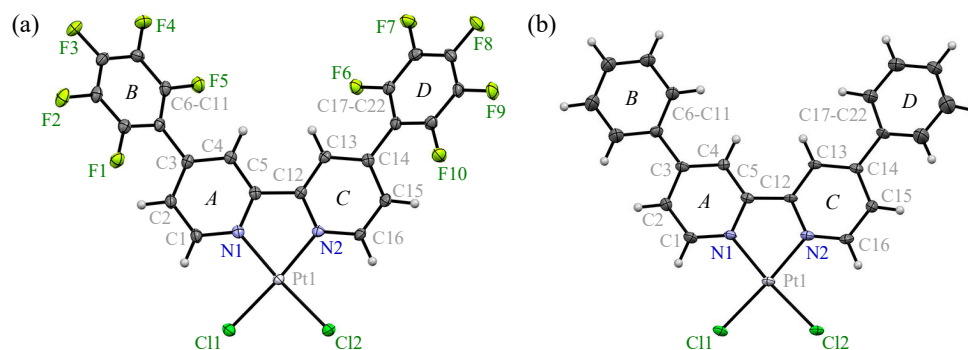

Figure 5. A part of crystal structures of (**a**) complex-1 in [PtCl$_2$**1a**]•CHCl$_3$ and (**b**) [PtCl$_2$**1b**] at 100 K, showing the atom-labeling schemes; displacement ellipsoids are drawn at the 50% and 30% probability levels, respectively.
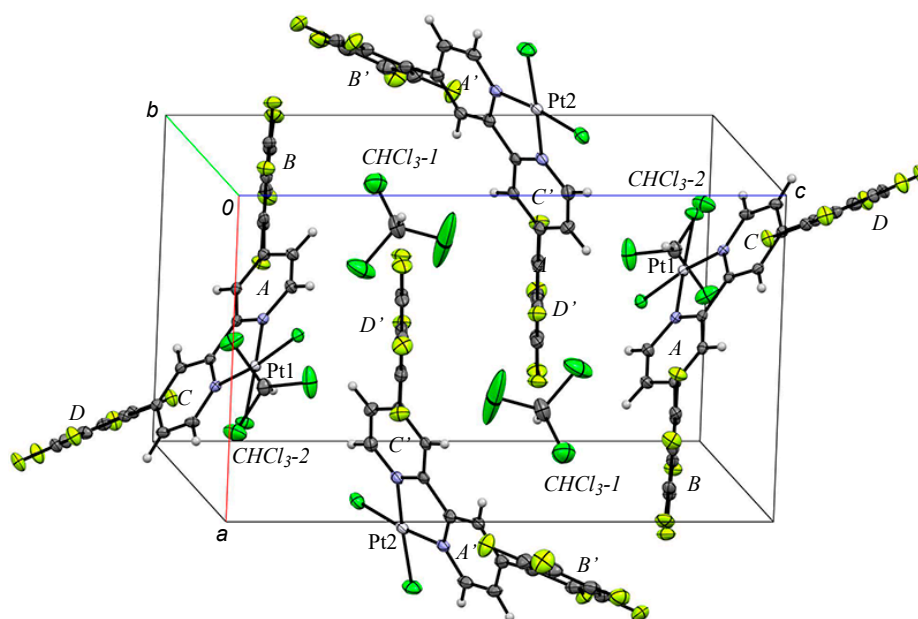

Figure 6. Part of the packing structure of [PtCl$_2$**1a**]•CHCl$_3$. Color scheme: C, gray; Cl, green; F, light green; N, blue.

In the crystal of [PtCl$_2$**1b**], the asymmetric unit contains the whole complex (Figure 5b). The geometry around the metal center is pseudo-square planar, and the bond distances of Pt1–N1, Pt1–N2, Pt1–Cl1, and Pt1–Cl2 are 2.010(8), 2.017(8), 2.307(2), and 2.306(3) Å, respectively. Two pyridine planes (*rings-A* and *-C*) are flat, and the torsion angle of N1-C5-C12-N2 is 1.5(13)°. With the phenyl groups (C6-C11, *ring-B* and C17-C22, *ring-D*) being approximately flat with respect to the corresponding pyridine rings, the dihedral angles between *rings A-B* and *C-D* are 6.19° and 9.60°, respectively, the improved planarity of the dihedral angles in [PtCl$_2$**1b**] compared to [PtCl$_2$**1a**] being consistent with the results suggested by the absorption spectra.

A part of the packing structure of [PtCl$_2$**1a**]●CHCl$_3$ is shown in Figure 6. The remarkable intermolecular interactions around Pt(II) centers are described below. Additional interactions of CH···Cl were observed between the bpy moiety and solvated CHCl$_3$ molecules and CF···π were observed between the pentafluorophenyl groups and the byp's π-plane, with 3.042(3), 3.339(3), and 3.042(3) Å for F2···C_g < *ring-C* > in complex-1, F9···C_g < *ring-C′* >, and F19···C_g < *ring-A′* > in complex-2, respectively. No specific π-hole···π interactions between the pentafluorophenyl rings and bpy moieties [39] were observed. For understanding the substitution of fluorine, a detailed analysis was performed, but CF···C_g < aromatic ring > was only observed for the bpy moieties due to the distorted conformation of the ligand.

Parts of the packing structures of [PtCl$_2$**1b**] are shown in Figure 7. In the crystal, two complexes form a dimer (Figure 7a), in which the complex [symmetry code: x, y, z] closely interacts with the adjacent complex^i [symmetry code: (i) x, y, −z + 1] with the π···π stacking between the two phenyl moieties. In this dimer, the intermolecular distance of Pt1 and Pt1^i is 11.143(1) Å. The *ring-B* (C6–C11) of the ligand closely interacts with the *ring-B^i* (C6^i–C11^i) of the adjacent complex^i; the distance of C_g < *ring-B* >···C_g < *ring-B^i* > is 3.770(8) Å, and the corresponding shortest perpendicular distance from the ring centroid to the adjacent plane is 3.602(6) Å. On the other hand, the distances of C_g < *ring-D* >···C_g < *ring-D^i* > and C_g < *ring-D* >···C_g < *ring-C^i* > are 4.680 Å and 4.491 Å, respectively, indicating the slippage and stacked conformation. Additionally, the shortest intermolecular distance of Pt1···Pt1′ is 6.2846(8) Å in the crystal, showing the dipole–dipole interactions as well as π···π stacking between the bpy moieties of [PtCl$_2$**1a**] (Figure 7b).
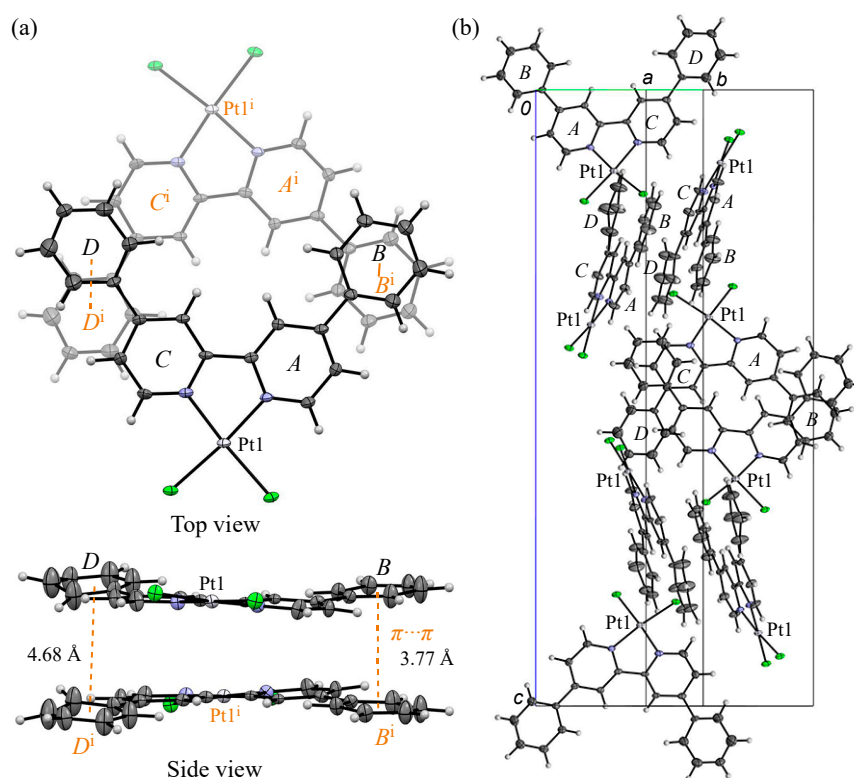

Figure 7. (**a**) Dimer and (**b**) packing structures of [PtCl$_2$**1b**]. Color scheme: C, gray; Cl, green; N, blue. Symmetry code: (i) x, y, −z + 1.

3.4. X-ray Crystallographic Study of [PtCl$_2$2]

The ORTEP views of the Pt(II) complexes in the crystal of [PtCl$_2$**2a**]●CH$_2$Cl$_2$ and [PtCl$_2$**2b**]●0.5C$_6$H$_6$ with the numbering schemes are shown in Figure 8. In the crystal of [PtCl$_2$**2a**]●CH$_2$Cl$_2$, the asymmetric unit contains a whole complex and one dichloromethane (see Figures 9a and 10). The complex comprises one Pt(II) ion, two Cl$^−$ ions, and one ligand

to give a mononuclear complex, [PtCl$_2$**2a**]. The geometry around the metal center is pseudo-square planar, and the bond distances of Pt1–N1, Pt1–N2, Pt1–Cl1, and Pt1–Cl2 are 2.012(2), 1.998(2), 2.2972(7), and 2.2872(7) Å, respectively. Two pyridine planes (*rings-A* and *-C*) are highly flat [the torsion angle of N1-C5-C14-N2 is −0.6(3)°] via Pt coordination. The pentafluorophenyl groups (C8-C9-C10-C11-C12-C13, ring-B and C21-C22-C23-C24-C25-C26, *ring-D*) are twisted with respect to the corresponding pyridine rings; the dihedral angles between *rings-A-B* and *C-D* are 6.25° and 28.13°, respectively.
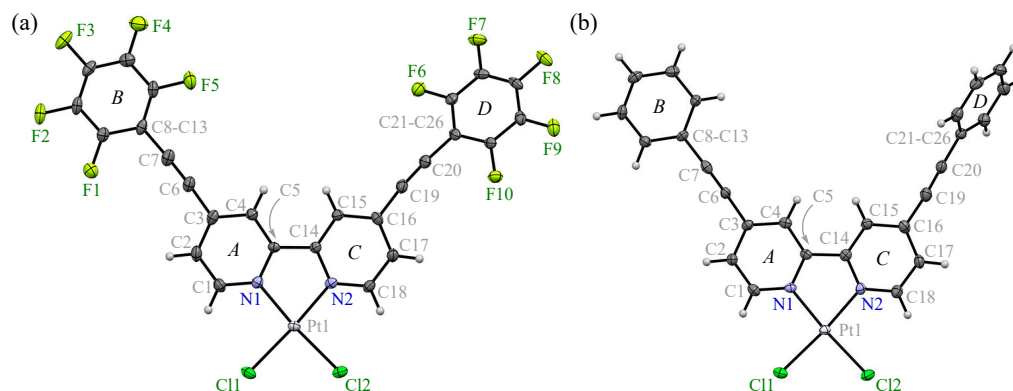

Figure 8. A part of crystal structures of (**a**) [PtCl$_2$**2a**]•CH$_2$Cl$_2$ and (**b**) [PtCl$_2$**2b**]•0.5C$_6$H$_6$ at 100 K, showing the atom-labeling schemes; displacement ellipsoids are drawn at the 50% probability level.
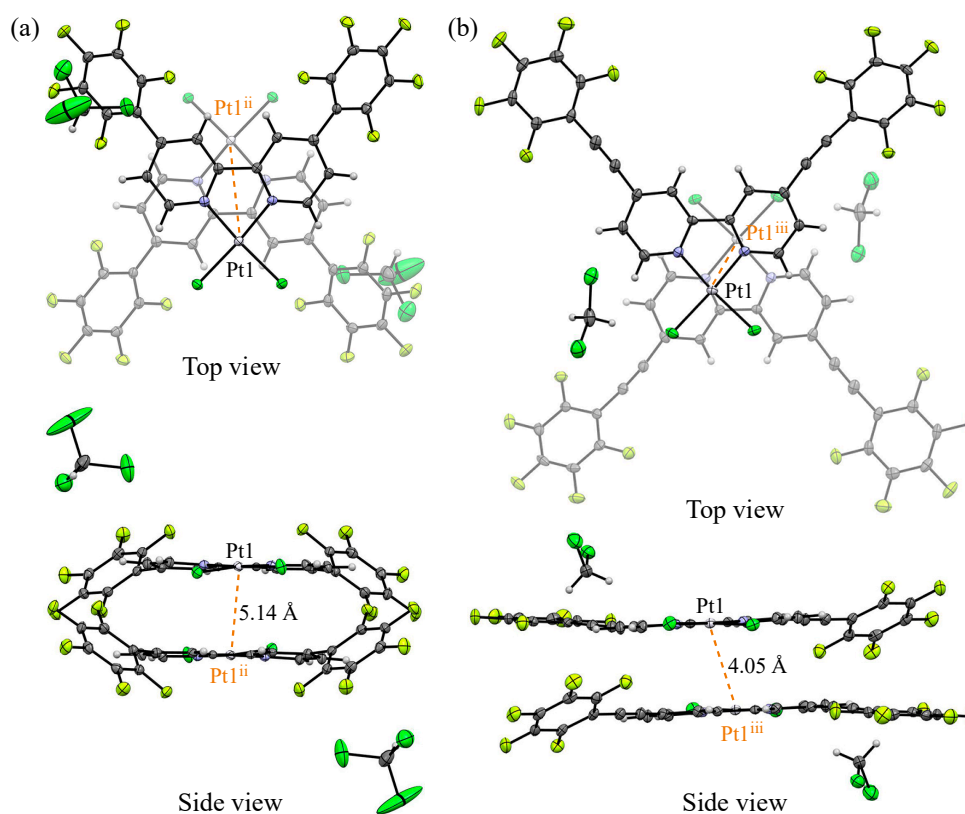

Figure 9. Views of the dimer structures of (**a**) [PtCl$_2$**1a**]•CHCl$_3$ and (**b**) [PtCl$_2$**2a**]•CH$_2$Cl$_2$. Color scheme: C, gray; Cl, green; F, light green; N, blue. Symmetry code: (ii) −x + 1, −y + 1, −z + 2, (iii) −x + 1.5, −y + 1.5, −z + 1.
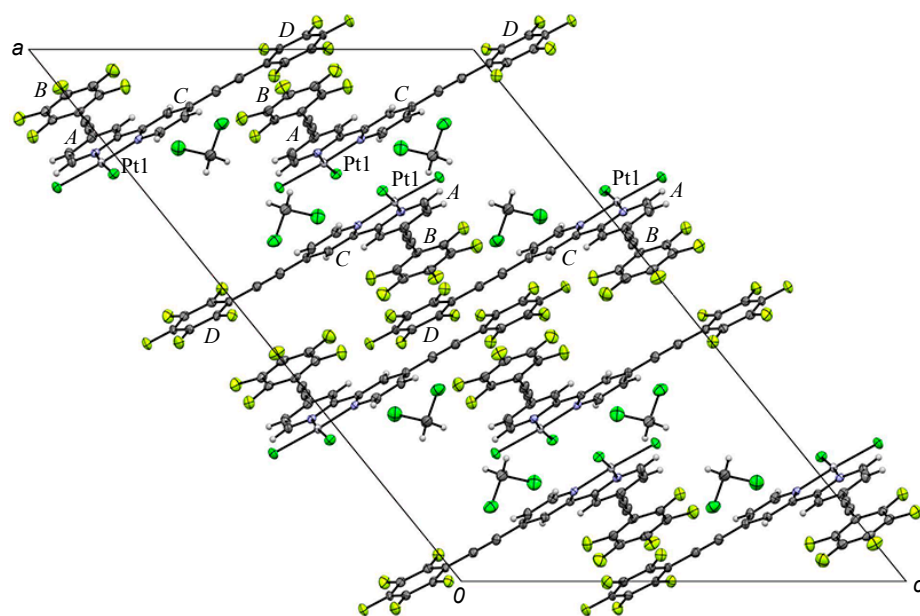
Figure 10. Part of the packing structure of [PtCl$_2$**2a**]•CH$_2$Cl$_2$. Color scheme: C, gray; Cl, green; F, light green; N, blue.

The dimer structures of two types of perfluorinated complexes, [PtCl$_2$**1a**] and [PtCl$_2$**2a**], are compared in Figure 9. The shortest intermolecular distance of Pt1···Pt1^{ii} (ii: −x + 1, −y + 1, −z + 2) in the crystal of [PtCl$_2$**1a**]•CH$_2$Cl$_2$ is 5.1370(7) Å (Figure 9a), and the corresponding Pt2···Pt2′ (−x+2, −y+1, −z+1) is 5.0066(7) Å to give the dimer through slipped π···π interactions of bpy moieties. The coordination five-membered rings also closely interacts through the π···π stacking; the intermolecular short distances of C_g < Pt1-N1-C5-C14-N2 >···C_g < Pt1^{ii}-N1^{ii}-C5^{ii}-C14^{ii}-N2^{ii} > and the corresponding complex-2 are 3.4661(19) and 3.412(2) Å, respectively. The dimer of [PtCl$_2$**2a**]•CH$_2$Cl$_2$ shows the same kinds of interactions (Figure 9b) and the shortest intermolecular distance of Pt1···Pt1^{iii} is 4.0513(9) Å. The related interaction between coordination five-membered rings is slightly separated through the slippage in the π···π stacking; the intermolecular short distance of C_g < Pt1-N1-C5-C14-N2 >···C_g < Pt1^{iii}-N1^{iii}-C5^{iii}-C14^{iii}-N2^{iii} > is 3.839(2) Å.

In the crystal of [PtCl$_2$**2b**]•0.5C$_6$H$_6$, the asymmetric unit contains a whole complex and one half of benzene (see Figure 11), indicating the isomorph structure of [PdCl$_2$**2b**]•0.5C$_6$H$_6$ [40]. The complex comprises one Pt(II) ion, two Cl$^−$ ions, and one ligand to give a mononuclear complex, [PtCl$_2$**2b**]. The geometry around the metal center is pseudo-square planar, and the bond distances of Pt1–N1, Pt1–N2, Pt1–Cl1, and Pt1–Cl2 are 2.005(3), 2.013(3), 2.2954(9), and 2.2931(10) Å, respectively. Two pyridine planes (*rings-A* and *-C*) are highly flat [the torsion angle of N1-C5-C14-N2 is 2.6(4)°] due to Pt coordination. The pentafluorophenyl groups (C8-C13, *ring-B* and C21-C26, *ring-D*) are twisted with respect to the corresponding pyridine rings; the dihedral angles between *rings-A-B* and *C-D* are 0.42° and 61.26°, respectively. The two complexes form a rhomb-like dimer with the inversion center through C-H···π interactions [6]; e.g., the complex [symmetry code: x, y, z] closely interacts with the adjacent complex^{iv} [symmetry code: (iv) −x + 2, −y + 1, −z + 1].

A benzene molecule, *ring-E*, is located in the rhomb-like framework, which is formed by the surrounded four phenylethynyl groups of the complexes. Two complexes are stabilized by CH···π interactions, and the intermolecular distance of C26-H26···C_g< *ring-B^{iv}* > is short (2.76 Å for H26···C_g < *ring-B^{iv}* > and 3.601(4) Å for C26···C_g < *ring-B^{iv}* >). The *ring-A* of the bipyridine closely interacts with the *ring-C^v* of the adjacent complex^v [symmetry code: (v) −x + 1, −y + 1, −z + 1]; the distance of C_g < *ring-A* >··· C_g < *ring-C^v* > is 3.449(2) Å and the corresponding shortest perpendicular distance from the ring centroid to the adjacent plane is 3.2638(14) Å. According to the π···π stacking, the intermolecular distance of Pt1 and Pt1^v is 6.5368(5) Å. A twisted phenyl *ring-D* further interacts with the

bipyridine moieties of the dimer, and the shortest distance of C_g < Pt1-N1-C5-C14-N2 >···C_g < *ring-D* > is 3.491(2) Å.
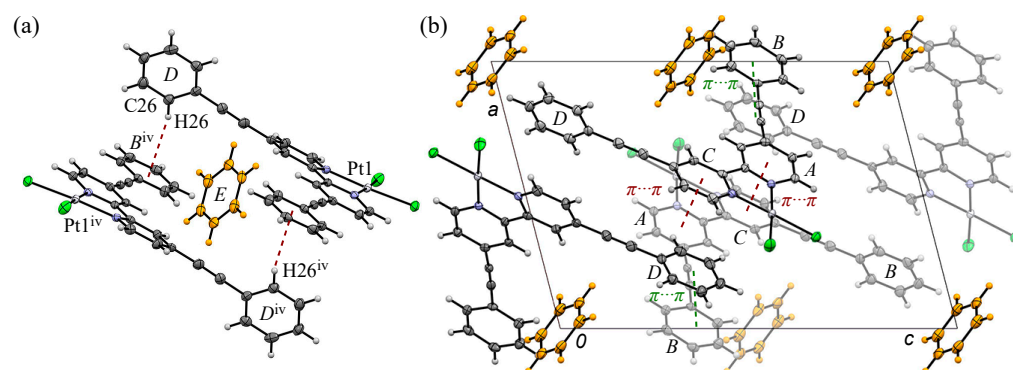

Figure 11. (**a**) The dimer and (**b**) packing structures of [PtCl$_2$**2b**]•0.5C$_6$H$_6$, showing the atom-labeling schemes. Displacement ellipsoids are drawn at the 50% probability level. Symmetry code: (iv) −x + 2, −y + 1, −z + 1.

3.5. Hirshfeld Surface Analysis of the Structures

To understand the detailed intermolecular interactions and the impact of fluorination on compound stability, the HS analysis [50,51] of each complex was carried out using Crystal Explorer 17.5 [52]. The analysis focused on [PtCl$_2$*L*] complexes, mapping the electron surface potential (ESP) with d_{norm} (the distance between the surface and external atoms) and generating fingerprint plots for the Pt and Cl atoms within each complex. The d_e (electron density) and d_i (distance inside) values ranged from 0.8 to 2.6 Å, as shown in Figure 12. The red spots observed in the d_{norm} plots represent short intermolecular distances within the molecules, indicating significant intermolecular interactions. Specifically, for the Pt(II) ion of [PtCl$_2$**1a**], the analysis highlighted the contributions from Pt···H (1.5%), Pt···C (0.6%), and Pt···N (0.1%) interactions. These findings suggest that the Pt(II) center primarily interacts with the hydrocarbon moiety of the bipyridine, without significantly enhancing the electron-rich regions of the molecule. Furthermore, for [PtCl$_2$**1b**], the predominant and specific interaction was found to be Pt···H (2.5%), which underscores the nucleophilic character of the Pt(II), demonstrating a preference for the positive ESP of protons. This characteristic is particularly noteworthy as it hints at the influence of fluorination on the molecule's electron-withdrawing properties and its subsequent effects on nucleophilicity.

The comparison between [PtCl$_2$**2a**] and [PtCl$_2$**2b**] revealed consistent patterns of interactions, with the fluorination of [PtCl$_2$**2a**] notably enhancing the intermolecular interaction between aromatic carbon atoms. This enhancement leads to a decrease in the metal's nucleophilic activity, facilitating closer stacking between the two metal centers—a phenomenon attributed to the electron-withdrawing nature of the fluorine substitutions.

These results collectively indicate that the introduction of a pentafluorophenyl group not only alters the electron density across the molecule, resulting in a positive shift of approximately 20 kJ mol^{-1} in the ESP (see Table 2), but also significantly impacts the molecular interactions at play. The increase in intermolecular interactions among the aromatic carbons, coupled with the reduced nucleophilic tendency of the metal, contributes to the overall stability of the fluorinated compounds. Through this detailed analysis, it becomes evident that fluorination plays a crucial role in modulating the physical properties and stability of these complexes, highlighting the nuanced balance between electron affinity, nucleophilicity, and intermolecular forces within the molecular structure.
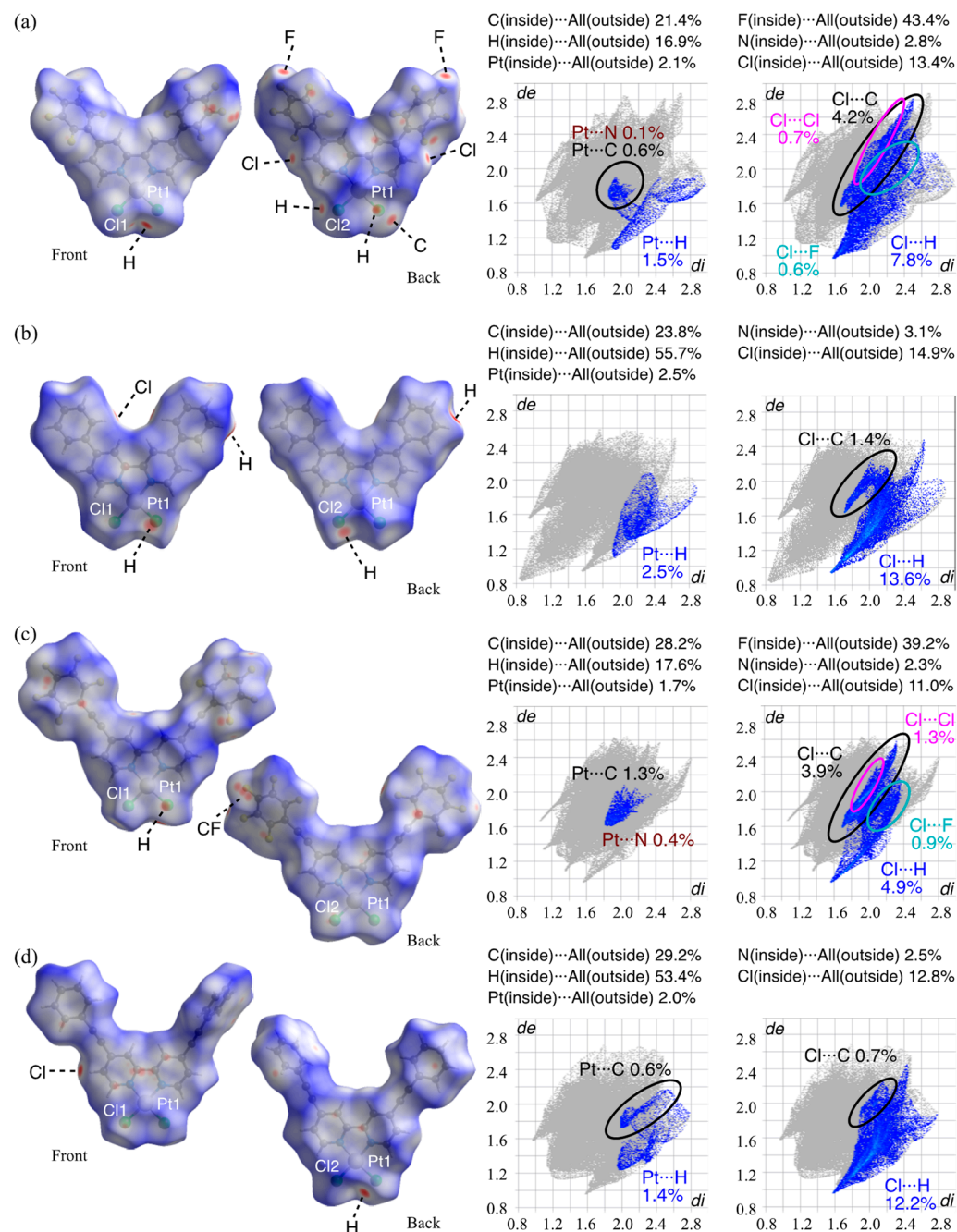
Figure 12. Comparison between fingerprint plot for the single molecule of [PtCl$_2$L] (L = **1** and **2**): (**a**) [PtCl$_2$**1a**], (**b**) [PtCl$_2$**1b**], (**c**) [PtCl$_2$**2a**], and (**d**) [PtCl$_2$**2b**], showing the d_e and d_i of 0.8–3.0 Å for all atoms and the metal ion.

4. Conclusions

In the realm of inorganic chemistry, the stacking of highly planar Pt(II) complexes within a crystal lattice is well documented to facilitate metallophilic interactions via the d orbitals of neighboring metal atoms. These interactions are pivotal for the development of color-sensitive materials. This study embarked on synthesizing such complexes, like [PtCl$_2$L], using bipyridine for its stable ligand complexing ability, and incorporated variants like [PtCl$_2$**1a**] with pentafluorophenyl groups and [PtCl$_2$**1b**] with phenyl groups. Additionally, our investigation extended to complexes [PtCl$_2$**2a**] and [PtCl$_2$**2b**], which feature an ethynyl linkage known to enhance ligand planarity. Contrary to expectations of orbital overlap, our findings indicated that the metals were separated by distances not conducive

to metal–metal interactions in both solid and solution phases. Nonetheless, a noteworthy formation of dimers was observed, characterized by overlapping ligands within the crystal structure. Notably, the phenyl group contributed to pronounced π-type interactions, while the pentafluorophenyl group introduced an intriguing aspect to crystal packing, potentially due to the inversion of the charge direction in the phenyl group's quadrupole moment. A detailed characterization of the fluorinated Pt(II) complexes, [PtCl$_2$**1a**] and [PtCl$_2$**2a**], revealed a dimeric arrangement with a shorter intermolecular metal-to-metal distance in the fluorinated complexes, highlighting the influence of fluorination; the shortest Pt···Pt interatomic distance in each dimer was 5.0066(7) and 4.0513(9) Å for [PtCl$_2$**1a**] and [PtCl$_2$**2a**], respectively, and that was 6.2846(8) and 6.5368(5) Å for [PtCl$_2$**1b**] and [PtCl$_2$**2b**], respectively. The theoretical band energy and ESP calculations by DFT, along with the electronic contribution of intermolecular interactions assessed through HS analysis, using the atomic coordinates from the corresponding crystal data were efficiently investigated to understand the crystal structures, and the results were also applied to understand the electronic states in solutions. This study contributes to a nuanced understanding of ligand planarity and metal interaction dynamics in complex formations, offering intriguing prospects for molecular design and crystal engineering.

Author Contributions: Conceptualization, validation, methodology, writing—review and editing, and funding acquisition, A.H.; writing—original draft preparation, A.H. and Y.T.; formal analysis, data curation, and investigation, Y.T., T.K., N.T. and T.H.; supervision, A.H. and H.Y. All authors have read and agreed to the published version of the manuscript.

Data Availability Statement: Crystallographic data have been deposited at CCDC, and additional data are available in Appendix A.

Conflicts of Interest: The authors declare no conflicts of interest.

Appendix A

Crystallographic data have been deposited with the Cambridge Crystallographic Data Centre, and the deposition CCDC numbers are 2346110-2346113 for [PtCl$_2$**1a**]•CHCl$_3$, [PtCl$_2$**1b**], [PtCl$_2$**2a**]•CH$_2$Cl$_2$, and [PtCl$_2$**2b**]•0.5C$_6$H$_6$, respectively. These data can be obtained free of charge via http://www.ccdc.cam.ac.uk/structures/ (accessed on 28 April 2024).

References

1. Williams, J.H. *Crystal Engineering, How Molecules Build Solids*; Morgan & Claypool Publishers: Kentfield, CA, USA, 2017.
2. Hunter, C.A. Meldola Lecture. The role of aromatic interactions in molecular recognition. *Chem. Soc. Rev.* **1994**, *23*, 101–109. [CrossRef]
3. Tsuzuki, S.; Fujii, A. Nature and physical origin of CH/π interaction: Significant difference from conventional hydrogen bonds. *Phys. Chem. Chem. Phys.* **2008**, *10*, 2584–2594. [CrossRef]
4. Wagner, J.P.; Schreiner, P.R. London dispersion in molecular chemistry-reconsidering steric effects. *Angew. Chem. Int. Ed.* **2015**, *54*, 12274–12296. [CrossRef]
5. Tiekink, E.R.T. Supramolecular assembly based on "emerging" intermolecular interactions of particular interest to coordination chemists. *Coord. Chem. Rev.* **2017**, *345*, 209–228. [CrossRef]
6. Yamada, S. Cation-π interactions in organic crystals. *Coord. Chem. Rev.* **2020**, *415*, 213301. [CrossRef]
7. Hirda, M. Fluorinated liquid crystals—Properties and applications. *Chem. Soc. Rev.* **2007**, *36*, 2070–2095. [CrossRef]
8. O'Hagan, D. Fluorine in health care: Organofluorine containing blockbuster drugs. *J. Fluor. Chem.* **2010**, *131*, 1071–1081. [CrossRef]
9. Gillis, E.P.; Eastman, K.J.; Hill, M.D.; Donnelly, D.J.; Meanwell, N.A. Applications of fluorine in medicinal chemistry. *J. Med. Chem.* **2015**, *58*, 8315–8359. [CrossRef]
10. Hori, A. *The Importance of Pi-Interactions in Crystal Engineering*; John Wiley & Sons: Hoboken, NJ, USA, 2012; pp. 163–185.
11. Nakajima, K.; Hori, A. Dynamic transformation and reversible guest encapsulations of pseudopolymorphs of a fully fluorinated β-diketonate Pd(II) complex. *Cryst. Growth Des.* **2014**, *14*, 3169–3173. [CrossRef]
12. Hori, A.; Gonda, R.; Rzeznicka, I.I. Enhanced adsorption of small gas molecules in metal (Cu^{2+}, Pd^{2+}, Pt^{2+}) complexes induced by ligand fluorination. *CrystEngComm* **2017**, *19*, 6263–6266. [CrossRef]

13. Ikumura, Y.; Habuka, Y.; Sakai, S.; Shinohara, T.; Yuge, H.; Rzeznicka, I.I.; Hori, A. Enhanced and heteromolecular guest encapsulation in nonporous crystals of a perfluorinated triketonato dinuclear copper complex. *Chem. Eur. J.* **2020**, *26*, 5051–5060. [CrossRef] [PubMed]

14. Ikumura, Y.; Habuka, Y.; Hori, A. Co-crystal structures and Hirshfeld surface analysis of mesitylene and/or *p*-xylene solvated pseudopolymorphs of fully fluorinated Pd(II) complex. *Polyhedron* **2021**, *197*, 115035. [CrossRef]

15. Reichenbächer, K.; Süss, H.I.; Hulliger, J. Fluorine in crystal engineering—"The little atom that could". *Chem. Soc. Rev.* **2005**, *34*, 22–30. [CrossRef] [PubMed]

16. Shimizu, K.; Gomes, M.F.C.; Pádua, A.; Rebelo, L.P.N.; Lopes, J.N.C. On the role of the dipole and quadrupole moments of aromatic compounds in the solvation by ionic liquids. *J. Phys. Chem. B* **2009**, *113*, 9894–9900. [CrossRef] [PubMed]

17. López, J.C.; Macario, A.; Maris, A.; Alkorta, I.; Blanco, S. How Aromatic fluorination exchanges the interaction role of pyridine with carbonyl compounds: The formaldehyde adduct. *Chem. Eur. J.* **2021**, *27*, 13870–13878. [CrossRef] [PubMed]

18. Mishra, B.K.; Arey, J.S.; Sathyamurthy, N. Stacking and spreading interaction in N-heteroaromatic systems. *J. Phys. Chem. A* **2010**, *114*, 9606–9616. [CrossRef]

19. Wang, H.; Wang, W.; Jin, W.J. σ-Hole Bond vs π-Hole Bond: A comparison based on halogen bond. *Chem. Rev.* **2016**, *116*, 5072–5104. [CrossRef] [PubMed]

20. Bauzá, A.; Frontera, A. σ/π-Hole noble gas bonding interactions: Insights from theory and experiment. *Coord. Chem. Rev.* **2020**, *404*, 213112. [CrossRef]

21. Pang, X.; Wang, H.; Wang, W.; Jin, W.J. Phosphorescent π-hole⋯π bonding cocrystals of pyrene with halo-perfluorobenzenes (F, Cl, Br, I). *Cryst. Growth Des.* **2015**, *15*, 4938–4945. [CrossRef]

22. Toikka, Y.N.; Mikherdov, A.S.; Ivanov, D.M.; Mooibroek, T.J.; Nadezhda, A.; Bokach, N.A.; Kukushkin, V.Y. Cyanamides as π-hole donor components of structure-directing (cyanamide)⋯arene noncovalent interactions. *Cryst. Growth Des.* **2020**, *20*, 4783–4793. [CrossRef]

23. Ibrahim, N.A.A.; Rady, A.S.M.; Al-Fahemi, J.H.; Telb, E.M.Z.; Ahmed, S.A.; Shawky, A.M.; Moussa, N.A.M. π-Hole interactions: A comparative investigation based on boron-containing molecules. *Chem. Select* **2020**, *5*, 13223–13231. [CrossRef]

24. Politzer, P.; Murraya, J.S.; Clark, T. The π-hole revisited. *Phys. Chem. Chem. Phys.* **2021**, *23*, 16458–16468. [CrossRef] [PubMed]

25. Toikka, Y.N.; Starova, G.L.; Suslonov, V.V.; Gomila, R.M.; Frontera, A.; Kukushkin, V.Y.; Bokach, N.A. Combined σ- and π-hole donor properties of perfluorinated iodo(or bromo)benzenes: Halogen bonding and π-hole Interactions in cocrystals including Cu$_4$I$_4$ Clusters. *Cryst. Growth Des.* **2023**, *23*, 5194–5203. [CrossRef]

26. Mallada, B.; Ondráček, M.; Lamanec, M.; Gallardo, A.; Jiménez-Martín, A.; de la Torre, B.; Hobza, P.; Jelínek, P. Visualization of π-hole in molecules by means of Kelvin probe force microscopy. *Nat. Commun.* **2023**, *14*, 4954. [CrossRef] [PubMed]

27. Yamanoi, Y. Recent Progress on the synthesis of bipyridine derivatives. *Molecules* **2024**, *29*, 576. [CrossRef] [PubMed]

28. Constable, E.C.; Housecroft, C.E. The early years of 2,2′-bipyridine—A ligand in its own lifetime. *Molecules* **2019**, *24*, 3951. [CrossRef] [PubMed]

29. Archer, S.; Weinstein, J.A. Charge-separated excited states in platinum(II) chromophores: Photophysics, formation, stabilization and utilization in solar energy conversion. *Coord. Chem. Rev.* **2012**, *256*, 2530–2561. [CrossRef]

30. Herber, R.H.; Croft, M.; Coyer, M.J.; Bilash, B.; Sahiner, A. Origin of polychromism of cis square-planar platinum(II) complexes: Comparison of two forms of [Pt(2,2′-bpy)(Cl$_2$)]. *Inorg. Chem.* **1994**, *33*, 2422–2426. [CrossRef]

31. Palmans, R.; MacQueen, D.B.; Pierpont, C.G.; Frank, A.J. Synthesis and characterization of bis(2,2′-bipyridyl)platinum(I): A novel microtubular linear-chain complex. *J. Am. Chem. Soc.* **1996**, *118*, 12647–12653. [CrossRef]

32. Katkova, S.A.; Mikherdov, A.S.; Sokolova, E.V.; Novikov, A.S.; Starova, G.L.; Kinzhalov, M.A. Intermolecular (isocyano group)⋯Pt^{II} interactions involving coordinated isocyanides in cyclometalated Pt^{II} complexes. *J. Mol. Struct.* **2022**, *1253*, 132230. [CrossRef]

33. Ni, J.; Guo, Z.; Zhu, Q.; Liu, S.; Zhang, J. The two-stepwise luminescent switching properties of triple-stimuli-responsive platinum(II) complexes bearing 4,4′-bis (2-phenylethynyl)-2,2′-bipyridine ligand. *Dye. Pigment.* **2023**, *217*, 111406. [CrossRef]

34. Jabbour, R.; Ashling, C.W.; Robinson, T.C.; Khan, A.H.; Wisser, D.; Berruyer, P.; Ghosh, A.C.; Ranscht, A.; Keen, D.A.; Brunner, E.; et al. Unravelling the molecular structure and confining environment of an organometallic catalyst heterogenized within amorphous porous polymers. *Angew. Chem. Int. Ed.* **2023**, *62*, e202310878. [CrossRef] [PubMed]

35. Sutton, J.J.; Preston, D.; Traber, P.; Steinmetzer, J.; Wu, X.; Kayal, S.; Sun, X.-Z.; Crowley, J.D.; George, M.W.; Kupfer, S.; et al. Excited-state switching in rhenium(I) bipyridyl complexes with donor−donor and donor−acceptor substituents. *J. Am. Chem. Soc.* **2021**, *143*, 9082–9093. [CrossRef] [PubMed]

36. Gavette, J.V.; Klug, C.M.; Zakharov, L.N.; Shores, M.P.; Haley, M.M.; Johnson, D.W. Intramolecular N–H⋯Cl hydrogen bonds in the outer coordination sphere of a bipyridyl bisurea-based ligand stabilize a tetrahedral FeLCl$_2$ complex. *Chem. Commun.* **2014**, *50*, 7173–7175. [CrossRef] [PubMed]

37. Calzolari, A.; Chen, Y.; Lewis, G.F.; Dougherty, D.B.; Shultz, D.; Nardelli, M.B. Complex materials for molecular spintronics applications: Cobalt bis(dioxolene) valence tautomers, from molecules to polymers. *J. Phys. Chem. B* **2012**, *116*, 13141–13148. [CrossRef]

38. Oppelt, K.; Egbe, D.A.M.; Monkowius, U.; List, M.; Zabel, M.; Sariciftci, N.S.; Knör, G. Luminescence and spectroscopic studies of organometallic rhodium and rhenium multichromophore systems carrying polypyridyl acceptor sites and phenylethynyl antenna subunits. *J. Organomet. Chem.* **2011**, *696*, 2252–2258. [CrossRef]

39. Hori, A.; Takatani, S.; Miyamoto, T.K.; Hasegawa, M. Luminescence from π–π stacked bipyridines through arene–perfluoroarene interactions. *CrystEngComm* **2009**, *11*, 567–569. [CrossRef]

40. Hori, A.; Ichisugi, R.; Azegami, D.; Toyama, N.; Yuge, H. Synthesis and crystal structures of rhomb-shaped dimeric Pd(II) complexes with arylethynyl-substituted 2,2′-bipyridine through CH···π interactions in the crystalline states. *Crystals* **2024**, *14*, 255. [CrossRef]

41. Frisch, M.J.; Trucks, G.W.; Schlegel, H.B.; Scuseria, G.E.; Robb, M.A.; Cheeseman, J.R.; Scalmani, G.; Barone, V.; Petersson, G.A.; Nakatsuji, H.; et al. *Gaussian 16, Revision C.02*; Gaussian, Inc.: Wallingford, CT, USA, 2016.

42. Takimiya, K.; Niihara, N.; Otsubo, T. Syntheses of 2-(pentafluorophenyl)thiophene derivatives via the palladium-catalyzed Suzuki reaction. *Synthesis* **2005**, 1589–1592. [CrossRef]

43. Sheldrick, G.M. SHELXT—Integrated space-group and crystal-structure determination. *Acta Cryst.* **2015**, *A71*, 3–8. [CrossRef]

44. Sheldrick, G.M. Crystal structure refinement with SHELXL. *Acta Cryst.* **2015**, *C71*, 3–8.

45. Osborn, R.S.; Rogers, D. Crystal structure of the red form of 2, 2′-bipyridyldichloroplatinum (II). *J. Chem. Soc. Dalton Trans.* **1974**, 1002–1004. [CrossRef]

46. Nishiuchi, Y.; Takayama, A.; Suzuki, T.; Shinozaki, K. A polymorphic platinum(II) complex: Yellow, red, and green polymorphs and X-ray crystallography of [Pt(fdpb)Cl] [Hfdpb = 1,3-Bis(5-trifluoromethyl-2-pyridyl)benzene]. *Eur. J. Inorg. Chem.* **2011**, *2011*, 1815–1823. [CrossRef]

47. Liu, R.; Chen, H.; Chang, J.; Li, Y.; Zhu, H.; Sun, W. Pt(II) diimine complexes bearing carbazolyl-capped acetylide ligands: Synthesis, tunable photophysics and nonlinear absorption. *Dalton Trans.* **2013**, *42*, 160–171. [CrossRef] [PubMed]

48. Yang, H.; Li, H.; Yue, L.; Chen, X.; Song, D.; Yang, X.; Sun, Y.; Zhou, G.; Wu, Z. Aggregation-induced phosphorescence emission (AIPE) behaviors in PtII(C^N)(N-donor ligand)Cl-type complexes through restrained D_{2d} deformation of the coordinating skeleton and their optoelectronic properties. *J. Mater. Chem. C* **2021**, *9*, 2334–2349. [CrossRef]

49. Watanabe, H.; Iwamura, M.; Nozaki, K. Kinetic Analysis of Excited-State Dynamics of Emissive Oligomers of Pt(II) Complex in Solution. *Inorg. Chem.* **2024**, *63*, 5580–5585. [CrossRef] [PubMed]

50. Spackman, M.A.; Jayatilaka, D. Hirshfeld surface analysis. *CrystEngComm* **2009**, *11*, 19–32. [CrossRef]

51. Hirshfeld, F.L. Bonded-atom fragments for describing molecular charge densities. *Theor. Chim. Acta* **1977**, *44*, 129–138. [CrossRef]

52. Turner, M.J.; McKinnon, J.J.; Wolff, S.K.; Grimwood, D.J.; Spackman, P.R.; Jayatilaka, D.; Spackman, M.A. *CrystalExplorer17*; University of Western Australia: Perth, Australia, 2017.